Digital Light Processing (DLP) of Nano Biphasic Calcium Phosphate Bioceramic for Making Bone Tissue Engineering Scaffolds

Yue Wang [1, 2], Shangsi Chen[2], Haowen Liang[1], Yang Liu[1], Jiaming Bai [1,*], Min Wang [2,*]

[1] Shenzhen Key Laboratory for Additive Manufacturing of High-performance Materials, Department of Mechanical and Energy Engineering, Southern University of Science and Technology, Shenzhen, 518055, China

[2] Department of Mechanical Engineering, The University of Hong Kong, Pokfulam Road, Hong Kong

---

* Corresponding Author:
[1] Professor Min Wang, at the University of Hong Kong, Hong Kong
Email: memwang@hku.hk Tel: +852 3917 7903 Fax: +852 2858 5415
[2] Professor Jiaming Bai, at the Southern University of Science and Technology
Email: baijm@sustech.edu.cn Tel: 0755-88015354

Abstract

Nano-sized ceramic particles are beneficial for the properties of 3D printed structures via digital light processing (DLP). However, achieving optimal conditions for the preparation and processing of ceramic nanoparticle-based slurry is a significant challenge. In this work, a stable and well dispersed slurry with nano-sized biphasic calcium phosphate (BCP) powders was developed and porous BCP bioceramic scaffolds with good bioactivity were accurately fabricated via the DLP additive manufacturing technology. Effects of dispersant, photoinitiator and solid loading on rheological properties and curing abilities of BCP slurries were systematically studied. The slurry having 65 wt. % of nano-sized BCP powders showed a relatively low viscosity of 400 mPa·s at the 50 s^{-1} shear rate. It was found that the optimal photoinitiator concentration was tightly associated with the energy dosage in DLP. Furthermore, the effects of sintering temperature (1100℃, 1200℃ and 1300℃) on the surface morphology, shrinkage, phase constitution, hardness, compressive properties, and *in vitro* biological performance of DLP-formed bioceramics were comprehensively investigated. The results showed that DLP-formed BCP ceramics sintered at 1300℃ had the best mechanical properties, *in vitro* cytocompatibility, and homogeneous bone-like apatite formation ability. Finally, DLP-formed 3D scaffolds with different pore sizes ranging from 300 μm to 1 mm were successfully fabricated, which exhibited high fidelity and accuracy. The current study has demonstrated the great potential of using DLP technology to construct functional complex BCP bioceramic scaffolds for bone tissue regeneration.

Keywords: nano-sized, biphasic calcium phosphate, digital light processing, sintering temperature

1. Introduction

Bone repair and regeneration has been in imperative demand owing to the increase of bone injuries caused by trauma, bone loss, and even congenital malformation, particularly for the defects that greater than the critical-sized bone defect (CSBD) which is difficult to heal spontaneously[1]. Bone tissue engineering (BTE) has flourished in recent years and showed great perspectives in biomedical field [2, 3]. Scaffold, as an essential component of scaffold-based tissue engineering, can give temporary structural support for cell attachment, growth, and proliferation, until the body has restored the basic functions of the host tissues[4]. So far, different types of materials have been tried for scaffolds, from metals, ceramics, and polymers to various composites[5, 6]. Among them, biphasic calcium phosphate (BCP), a mixture of hydroxyapatite (HAp) and β-tricalcium phosphate (β-TCP), is an excellent bioceramic for hard tissue repair due to its hybrid advantages of HAp and β-TCP[7, 8]. HAp is chemically similar to the inorganic composition of native hard tissues such as bone and teeth. It processes excellent biocompatibility, bioactivity, and osteoconductivity, thus is widely used in clinical bone repair [9-12]. However, the biodegradation rate of HAp is often slow, which leads to a long degradation period and restricts the bone regeneration process[13]. β-TCP is a popular bioresorbable bioactive ceramic material that can be absorbed and transformed into new bone tissues though continuous cell metabolism[14, 15]. Therefore, the combination of HAp and β-TCP has been considered as a desirable biomaterial for bone tissue engineering scaffold and numerous studies have demonstrated their efficacy[16-18].

Liu *et al.* fabricated BCP scaffolds with controlled macro-pore size and porosity and the *in vivo* implantation exhibited that they had excellent mechanical properties and bone-forming abilities [19]. Bouler *et al.* detailedly reviewed the biological responses of BCP-based materials for biomedical use and demonstrated the great future applications as osteoconductive scaffold[7].

For bone tissue engineering scaffolds, several requirements should be fulfilled, such as biocompatibility, biodegradability and sufficient mechanical property [20]. Furthermore, scaffolds should also have highly porous structures with interconnected pores, which are beneficial for nutrient and oxygen transport, thus promoting tissue regeneration. Conventional fabrication methods such as thermally induced phase separation, freeze drying, solvent casting, and electrospinning have been investigated for manufacturing tissue engineering scaffolds [21, 22], however, scaffolds fabricated by these conventional approaches present inevitable problems, including uncontrollable pore size or incomplete pore interconnectivity [23].

Recently, additive manufacturing(AM), also popularly named 3D printing, has emerged and considered as a powerful platform for fabricating tissue engineering scaffolds [24, 25]. Several AM technologies have been employed for bioceramic fabrication in tissue engineering field, such as stereolithography (SLA), binder jetting (BJ), direct ink writing (DIW), selective laser sintering (SLS), and digital light processing (DLP) [26-28]. Among these various AM technologies, DIW plays a vital role in ceramic fabrication for biomedical application owing to its low cost, easy operation, and wide materials available[29]. Alumina, zirconia, bioglass, and calcium phosphate based bioceramics have been widely reported for implant/scaffold

fabrication[30-32]. However, the resolution and dimensional accuracy are insufficient for complex structures with small features[33]. DLP is one of the most promising approaches to construct complex ceramic parts with high resolution and accuracy, as well as desirable mechanical properties[26, 34, 35].

To fabricate ceramic scaffolds via DLP, ceramic particles are added to the resin medium for the preparation of photo-curable ceramic slurry. Polymerization reactions within resin matrix will be initiated when exposed to laser or UV light. The ceramic particles will be surrounded by the cross-linked polymer in the printing[36, 37]. After thermal debinding and sintering, the polymer binders will be removed, and then pure ceramic parts will be obtained. Two key points should be considered in this process. One is to avoid the cracks caused by the thermal treatment[38]. Therefore, slurry with high solid loading is needed[39]. However, with the increase of the solid loading of ceramic slurries, the viscosity rises rapidly. It is unfavorable for the self-leveling of new layers in the printing process, which results in the printing failure, especially for the DLP machines without recoating blades[40]. Furthermore, nano-sized ceramic particles are proved to be beneficial for improving mechanical properties of the final parts, although obtaining ceramic slurry with high solid loading has more difficulties since nano-sized particles have high specific surface area and surface energy that are easy to agglomerate with surrounding particles[41]. Therefore, developing slurries containing nano-sized ceramic particles with high solid loading and low viscosity are essential in ceramic DLP process[42]. Also, achieving optimal conditions for the DLP processing of ceramic nanoparticle based slurry remains a challenge owing to the light scattering caused by the ceramic particles[43]. The other is the effect of different

sintering temperature on the properties of final ceramic parts. For bioceramic fabrication, sintering temperature is tightly related to the surface morphology, porosity, volume density, and mechanical properties of the samples and further influences the biological behaviors[44]. Especially for BCP ceramics, phase transformation may occur in the sintering process[45, 46]. However, few studies have systematically studied the effects of sintering temperature on the properties of BCP bioceramics prepared by DLP AM technology.

In the present work, nano-sized BCP ceramic slurry with 65 wt.% solid loading was prepared and processed via DLP AM technology. The effects of dispersion, photoinitiator concentrations on the rheological properties and polymerization behaviors of the BCP slurry were studied. Subsequently, the effects of different sintering temperatures on surface morphology, shrinkage, phase stability, mechanical properties, and *in vitro* biological responses of DLP-formed bioceramics were investigated. Furthermore, high-performance DLP-formed BCP scaffolds were fabricated using the optimal sintering temperature. Our results have provided insights for the fabrication of high-performance BCP BTE scaffolds by the emerging AM technology.

2. Materials and Methods

2.1 Materials

The HAp powders (needle-like shape; diameter: 20 nm; length: 270 nm) and β-TCP powders (near-spherical shape; d50: 500 nm) were provided by Nanjing Emperor Nano Material Co., LTD. 1,6-hexanediol diacrylate (HDDA) as the monomer was obtained from Shanghai Yinchang New Material Co., Ltd. Diphenyl

(2,4,6-trimethylbenzoyl) phosphine oxide (TPO, Aladddin) was used for initiating the photo-polymerization. Three types of dispersants, BYK111 (phosphoric acid ester), BYK2055 (Modified polyacrylate) (BYK Chemie, Germany), and monoalcohol ethoxylate phosphate (MAEP) (Kelon Chemical Reagent Factory, Chengdu, China) were selected for surface modification of BCP powders. Fetal bovine serum (FBS), Dulbecco's Modified Eagle Medium (DMEM), and penicillin-streptomycin were purchased from Gibco (Thermo Fisher Scientific, USA). Live-dead assay kit was provided by Invitrogen (Thermo Fisher Scientific, USA). All materials and reagents were used as received without further processing.

2.2 Surface modification of BCP powders

Three types of dispersants with the concentration of 5.0 % relative to the weight of BCP powders were applied for surface modification of the ceramic particles. Same weight of HAp and β-TCP powders (HAp: β-TCP=1:1) were dried at 80℃ for 12h to avoid any moisture. Then, the dispersant was added to ethanol solution. After full dissolution of the dispersant, ceramic particles were mixed thoroughly with the dispersant solution via a turbula shaker mixer (Turbula T2F, Basel, Switzerland) for 12h. The ceramic solution was then dried in an oven at 60℃ for 48h. After crushing and screening with a 60-mesh sieve, the modified BCP powders were obtained. The rheological properties of 40 wt. % BCP slurry with modified powders were evaluated and compared. Afterwards, the better dispersant with different concentrations (1.0%, 3.0%, 5.0%, 8.0%, 9.0%, 10.0%, 12.0%, and 15.0%) relative to the weight of BCP powders were prepared in the same way to obtain the optimal ratio of the dispersant for BCP powder modification.

2.3 TPO concentration optimization and slurry preparation

Photoinitiator is an essential component in the photo-curable slurry. It can absorb sufficient energy to initiate the polymerization and thus have a close relationship with the curing abilities of the slurry. Therefore, the effect of TPO concentration on cure depth was investigated. Different TPO amounts ranging from 0.5 wt. % to 2.0 wt. % relative to the mass of resin weight were employed for BCP slurries with 40 wt. % solid loading.

Then, the photo-curable resin was prepared by mixing HDDA and TPO with specific concentration. Whereafter, modified BCP powders were added in the resin matrix and mixed by planetary ball milling machine with the speed of 400r/min for 12h to obtain stable and homogenous slurry. In this context, suspensions with different solid loading (50 wt.%, 60 wt%, 65 wt%, 70 wt.%, and 75 wt.%) were prepared [40].

To obtain the optimal printing parameters, curing abilities of the ceramic slurry should be evaluated. Cure depth reflects the curing behavior under the given energy and is required several times larger than the layer thickness to avoid insufficient interlayer combination. Generally, the cure depth is influenced by the total energy input according to the Jacobs equation[36]:

$$C_d = D_p \ln\left(\frac{E}{E_c}\right) - - - - - - - - - - - - - (1)$$

where C_d is the cure depth, D_p is the penetration depth when the light intensity is reduced to 37%, E is the energy input, E_c is the critical energy. Based on the experimental data of C_d at different E, the relation between C_d and E can be

obtained through linearly fitting to Jacobs equation. That equation could provide a guidance for parameter selection in the printing.

2.4 Fabrication of BCP ceramic parts via DLP

The BCP green parts were fabricated by a commercial bottom-up DLP printer (Asiga Max, Australia), which is capable of adjusting the energy density, exposure time, and layer thickness. First, the standard stereolithography (STL) file was prepared and transferred. When printing started, the printing platform positioned one layer thickness above the bottom of the resin tank. Second, the UV light selectively exposed to the resin surface and cured one-layer slurry based on the slicing data. Third, the printing platform uplifted and made the cured parts detach with the transparent substrate. The platform lowered again after the slurry self-leveling and started the next-layer printing. The process repeated layer by layer, until the entire part was fully completed. Finally, the green body was ultrasonically cleaned with ethanol to remove the uncured slurry.

To determine the optimal debinding parameters and obtain the crack-free BCP scaffolds, thermalgravimetric analysis (TGA) (Discovery, TA Instruments, USA) was conducted with heating from 30℃ to 700℃ in a nitrogen atmosphere at a rate of 10℃/min. Based on the TGA result, an optimized debinding and sintering strategy were used to obtain the final BCP bioceramic in a muffle furnace, the scheme of BCP fabrication via DLP AM technology is shown in Fig.1.

2.5 Characterization

The rheological property was performed via a rheometer (MCR-92, Anton Paar, Australia). Shear rate ramped from 0 s^{-1} to 100 s^{-1}. The cure depth was obtained

through controlling the first exposure and measured by a digital micrometer (Mitutoyo MD-25PX, Japan). The surface microstructure and morphology of sintered ceramics were observed by a scanning electron microscopy (SEM, ZEISS Merlin, Germany) with an acceleration voltage of 5KV. The phase composition was confirmed by X-ray diffraction (XRD, Rigaku Smartlab, Japan) at a scanning rate of 10°/min from 20° to 60°. The mass fraction of the main phase was calculated via adiabatic method. If the samples include two phases A and B, the mass fraction can be calculated by the following equation (2)[47]:

$$W_A = \frac{I_A}{I_A + \frac{I_B}{K_A^B}} \quad ; \quad W_B = \frac{I_B}{I_B + I_A * K_A^B} \quad ; \quad K_A^B = \frac{RIR_B}{RIR_A} \text{---------(2)}$$

Where W is the mass fraction, I is the integrated intensity of the strongest peak of the phase (the area of the strongest peak), RIR is the reference intensity ratio and can be found in the PDF card ($RIR_{HAp} = 1.10, RIR_{\beta-TCP} = 1.20$) [48].

The shrinkage was calculated according to the equation (3)[49]:

$$\mathrm{S} = \frac{Y - L}{L} * 100\% \text{-----------(3)}$$

where S is the linear shrinkage, L is the size after sintering, Y is the designed size of the model.

The open porosity of scaffolds was determined using the Archimedes method by employing an electronic analytical balance (FA2104J, Sunny Hengping Scientific Instrument, Shanghai). The weight of scaffolds in the dry state was measured as M_d. Then, the scaffolds were immersed in ethanol in a beaker which was put in a vacuum chamber for 10 min to force out the trapped air in the pores. The scaffolds were

removed from ethanol and filter paper was used to remove the ethanol from the surface. The weight of the wet scaffolds was measured in the air as M_w while M_l denoted the weight of the submerged scaffold. The porosity was calculated by the equation below [50]:

$$Porosity(\%) = \frac{M_w - M_d}{M_w - M_l} * 100\% \quad (4)$$

The bulk volume density of the sintered disk (Φ10×2mm) was obtained following the equation (5):

$$Volume\ density = \frac{M_d * \rho_l}{M_l - M_d} \quad (5)$$

Where ρ_l is the density of the liquid (ethanol). Five samples were tested for open porosity and volume density for an average, respectively.

Compressive strength of porous cubic structure with 58 vol.% porosity (dimensions: 5.4×5.4×5.4 mm, pore size: 1 mm; square pore) was studied by a universal testing machine (TST-C1019, 0-2 kN, China) with the loading speed of 1mm/min. Five samples were tested for an average. The hardness of the solid disks (Φ10×2 mm) was evaluated through Vickers hardness tester (HXD-1000TMC/LCD, China) and the load was 200 g with dwell time 20 s. Five samples and five regions for each sample were tested. The surface roughness of the sintered samples (Φ10×2 mm) was characterized through a laser scanning confocal microscope (VK-X1000, KEYENCE, Japan). Three samples were tested in five regions.

2.6 *In vitro* biological evaluation of BCP bioceramics

Rat bone mesenchymal stem cells (BMSCs) derived from bone marrow were used to evaluate the biological behavior of DLP-formed BCP bioceramics (bulk disks:

Ø6×1 mm). To explore the cell proliferation behavior on BCP ceramics, BMSCs at a density of 1.0×10^3 cells/well were seeded on three types of BCP ceramics and blank culture plate (control group) in 96-well cell culture plate and cultured with DMEM medium in an incubator supplemented with 5% CO_2 at 37℃. After culturing for 1, 3, and 5 days, the cell viability was performed by MTT assay.

To evaluate cell survival and attachment on the BCP bulk disk samples, BMSCs at a density of 5.0×10^3 cells/well were seeded. After incubation for 4 h and 24 h, the live/dead assay was used to study the cell survival and adhesion on BCP ceramics. After staining, the cells were observed with a fluorescence microscope (Leica DMi8, Germany). The living cells were stained green, and the dead cells were red when exposed to relative fluorescence. Besides, after 24 h of culture, BCP samples were fixed by 4% polyformaldehyde (Sigma-Aldrich, USA) for 20 min and then washed with PBS twice. Subsequently, BCP samples were dehydrated in a graded ethanol series from 30, 50, 60, 70, 80, 90, 100% ethanol for 10 min each. The samples were then dried at room temperature, and then sputter coated with gold for SEM observation.

2.7 Bioactivity evaluation

To evaluate the bioactivity of the DLP-formed BCP bioceramics, the samples were soaked in the simulated body fluid (SBF, Shanghai yuanye Bio-Technology Co., Ltd, Shanghai, China) for 72 h in 37℃ water bath. Afterwards, the samples were washed with deionized water and dried at 60℃ for 6 h. Then, SEM was used to observe the apatite formation on the ceramic surface. Besides, the chemical composition towards the formation layer was investigated by Energy Dispersive X-

Ray Spectroscopy (EDS).

2.8 Statistical analysis

All quantitative data were obtained through three or five parallel samples and presented as mean value ± standard deviation. The hardness, compressive strength, and MTT assay result were analyzed using one-way ANOVA. Significant difference was set as $p < 0.05$(*).

3. Results and discussions

3.1 Study of the dispersants

To obtain a stable and well dispersed BCP ceramic slurry, the dispersant plays a key role, which was studied comprehensively in this work. Fig.2 shows the viscosities of 40 wt.% solid loading BCP ceramic slurries with (a) different dispersant types and (b) BYK111 with various concentrations ranging from 1.0 wt.% to 15.0 wt.%. Obviously, slurries with BYK111 modified powders had the lowest viscosity compared to other dispersants, indicating it should be used for the following preparation of the photo-curable slurry. This is might due to the anchoring head of the phosphate group in the BYK111, making it easily combine with the BCP particles while polymer chain at the other side provides the affinity to non-aqueous media. It leads to a thick steric barrier layer on the surface of the ceramic particles and forms the sufficient repulsive force between the surrounding ceramic powders, which exhibits the best dispersion effects [51, 52]. Furthermore, it was observed that the optimal ratio for BYK111 modified BCP ceramic powders was 9.0 wt. % from Fig.2(b). When the dispersant amount was less than 9.0 wt. %, the ceramic powders were insufficient dispersed and had a higher viscosity. However, when the dispersant

exceeded the optimal ratio, slurry viscosities slightly increased, which indicated the rheological property of the slurry deteriorated. This might be attributed to the addition of excessive dispersants. If the unreacted dispersants overcame a threshold, they remained free in the slurry and a flocculation related to osmotic effects could occur which damaged the stability of the slurry and increased the viscosity [53, 54].

3.2 The optimal amounts of TPO and properties of ceramic slurries

The effect of TPO concentration on the cure depth of the slurry at different energy input is shown in Fig.3 (a). The cure depth was positively correlated with energy dose for a given TPO concentration owing to the high energy absorbed of the system. Besides, as the energy dose increased, the location of the optimal TPO concentration moved forwards lower concentration. The results showed a good agreement with Lee's work[55]. Lee *et al.* investigated the cure depth of pure resin system as a function of photoinitiator concentration in both experimental and theoretical side. The proposed equation illustrated that the critical photoinitiator concentration was closely associated with the energy dosage. With the photoinitiator concentration raising, the penetration depth of the photons decreases, thus reducing the free radical initiation. The current results indicated that the addition of the ceramic particles did not affect this rule and can be applied to the ceramic slurry system for DLP printing.

Fig.3 (b) shows the rheological behaviors of 50 wt.%, 60 wt.%, 65 wt.%, 70 wt.%, and 75 wt.% BCP ceramic slurries as the function of shear rates. All these slurries showed a shear thinning behavior that was beneficial for the printing and

storing. In this study, 65 wt.% solid loading was employed for the following printing owing to its fast self-leveling speed and sufficient printing accuracy. The optimized nano-sized BCP slurry with 65 wt.% solid loading showed competitive lower viscosity of 400 mPa·s at 50 s^{-1} shear rate [9, 56]. The curing ability of 65 wt.% slurries was studied as shown in Fig.3(c). After data fitting to the Jacobs equation, the relationship between cure depth and exposure energy for 65 wt.% BCP slurry can be described by equation (6), which can be used for selecting suitable printing parameters for the printing.

$$C_d = 150.1 * \ln\left(\frac{E}{5.0}\right) \quad (6)$$

Considering the cure depth-energy dose equation, 20 mJ/cm^2 energy dose with TPO concentration 1 wt.% relative to the mass of resin weight was employed in this study. The final formulation of BCP slurry contained 65 wt.% BCP powders (HAp: β-TCP=1:1), 5.85 wt.% BYK111 (9 wt.% relative to weight of BCP powders), 28.86 wt.% HDDA, and 0.29 wt.% TPO (1 wt.% relative to weight of resin).

TGA was performed to analyze the thermal decomposition of the green part and guide the profile of the debinding process, as shown in Fig. 4(a). It can be found the mass loss mainly happened between 300 and 500 ℃. The 435℃ peak indicated the fast decomposition of the photosensitive resin. Therefore, the debinding and sintering profile was set as shown in Fig.4b. Originally, a heating rate of 1℃/min was used before 300 ℃. Then, heating to 500℃ at a slow heating rate of 0.15 ℃/min. Afterwards, the heating rate increased to 1℃/min. All the printed samples kept at 435℃ and 600 ℃ for 3h. After debinding, the samples of BCP ceramics were divided into three groups and sintered at 1100℃, 1200℃, and 1300℃ at 2 ℃/min,

respectively.

3.3 Shrinkage, density, and microstructure

The sintered ceramics fabricated via DLP process will undergo inevitable shrinkage during sintering[57]. Understanding the shrinkage and dimensional accuracy is important to predict the dimensional difference between 3D design and final products. A cylinder was tested in current work and the size of the tested samples in the X-Y and Z dimensions was shown in Table1. Shrinkages of X-Y and Z direction of the sintered-1100 BCP ceramics were 6.5% and 6.0%, respectively. After sintering at 1200℃, there was a huge increase of the shrinkage in three directions, ~16.2% in X-Y plane and 17.0% in Z direction. This indicated that the ceramic particles begun to tightly interconnect with surrounding ceramic particles and the ceramics became denser when heated from 1100 to 1200℃. The SEM observation (Fig.5 a-b) and volume density value also demonstrated the shrinkage changes. After sintering at 1300℃, the sintered BCP ceramics became much denser without any voids and the particles were tightly interconnected with all grains (Fig.5c), demonstrating a high level of densification were obtained. It was shown that the shrinkage was approximately equal in three dimensions at ~22% after sintering at 1300℃, suggesting a near-isotropic shrinkage which may effectively avoid cracking in the thermal treatment. Fig.5d shows the volume density of the sintered scaffolds. The volume density of the scaffolds after sintering at 1100 ℃, 1200℃, and 1300℃ was 2.780 ± 0.010, 2.935 ± 0.012, and 3.037 ± 0.009 g/cm^3, respectively. With the increase of the sintering temperature, the volume density increased obviously. This result was in good agreement with the microstructure analysis.

3.4 Surface roughness

Surface roughness of substrate is tightly related to the cell behaviors and has a direct influence on cell adhesion, proliferation, and phenotype expression [58-60]. Fig.6 shows the 3D topography images and surface roughness values of the sintered parts. The top surface is the side closed to the building platform while the bottom surface is the final cured layer. The top surface is rougher than the bottom surface because the roughness of top side depends on the quality of the building platform and a rough platform surface is beneficial for the attachment of the first layer. The bottom surface reflects the true curing surface quality of the sintered parts. Generally, the surface roughness of the sintered disks treated by three sintering temperatures (1100℃, 1200℃, and 1300℃) had no significant difference. With the sintering temperature increasing, the surface roughness of obtained parts slightly decreased. The samples sintered at 1300℃ exhibited a smoother surface roughness, which was mainly owing to its denser microstructures without any voids. Hatano *et al.* suggested osteoblasts attached and proliferated more effectively when the surface roughness of the substrate was about 0.8μm[61]. Therefore, in current study, the BCP ceramics sintered at the range of 1100℃-1300℃ could be also beneficial for cell behaviors.

3.5 Phase constitution

The phase constitution of the sintered parts is closely related to the physicochemical properties of the scaffolds. Fig.7 displays the XRD pattern of the sintered BCP samples at 1100℃, 1200℃, and 1300℃. After sintering, the strong peaks of HAp (0,0,2) (2,1,1) (1,1,2) and β-TCP (2,1,4) (0,2,10)(2,2,0) were detected

without any secondary phases which were in accordance with Lee's work[62]. There were no standard peaks of α-TCP, showing the transformation of β-TCP to α-TCP was not occur[63]. The absence of the resin and dispersant demonstrated the purity of the sintered ceramic. Furthermore, the mass fraction of the HAp after sintering at 1100, 1200, and 1300℃ was 54.1±0.3%，46.9±1.0%，and 45.9±1.9%, respectively. As the sintering temperature increased, the ratio of HAp to β-TCP decreased, indicating the phase transition from HAp to β-TCP was occur after thermal treatment. Overall, the XRD results indicated that the HAp was not much decomposed after sintering and could offer excellent bioactivity for bone tissue engineering applications.

3.6 Mechanical properties

An ideal scaffold should have desirable mechanical properties and maintain structural integrity until the targeted tissues restore their inherent functions and properties. The hardness and compression strength are two essential factors to evaluate whether the implants or scaffolds are suitable for the loading-bear application in clinic. Fig.8(a) shows the Vickers hardness of the sintered BCP ceramic disks. It was seen that the hardness of 1300℃-sintered samples was 6.36±0.43 GPa. To evaluate the compressive strength of porous BCP scaffold for BTE application, 58 vol.% porosity of the cubic-shaped scaffold was designed and printed via DLP AM technology. After printing, the porosity of the green bodies was 55.1±2.2%. The decrease of the porosity after printing as compared to 3D models was because of the light scattering in the photopolymerization. After sintering at three temperatures,

their porosities were 68.4±2.1%, 60.9±1.4%, and 56.3±2.8%, respectively. The differences were mainly attributed to the microstructure of the sintered ceramics. Fig.8(b) shows the compressive strength of the porous cubic scaffolds. It was seen that the compressive strength values of 1300℃-sintered samples reached 20.07±2.09 MPa. Generally, as the sintering temperature increased, both the hardness and compressive strength dramatically increased, which indicated after sintering at 1300℃, the BCP ceramics had the best mechanical properties. This could be explained by the high densification of the BCP particles in the 1300℃-sintered samples. The compressive strength of human cancellous bone is about 1.5-45 MPa [64], and the hardness of human bone is associated with its composition, porosity, and structures. In current study, the BCP scaffolds sintered at 1300℃ with about 56.3 vol.% porosity presented comparable mechanical properties with human cancellous bone, which seemed that it could be possible for bone tissue engineering application.

3.7 *In vitro* biological properties of BCP bioceramics

The BMSCs were used to evaluate the *in vitro* biological behaviors of the sintered BCP bioceramics. Fig.9 shows the cell proliferation rate of BMSCs cultured on the DLP-formed BCP ceramics for 1, 3 and 5 days. BCP samples sintered at 1100, 1200, and 1300℃ showed similar cell proliferation rates with the blank control, which indicated that BCP ceramics were biocompatible and could provide a suitable environment for cell growth. Furthermore, BCP samples sintered at 1300℃ showed the highest OD value in comparison with BCP samples sintered at 1100℃ and 1200℃,

suggesting that BCP ceramics sintered at 1300℃ performed a better cell response. This could be attributed to the higher stiffness of BCP ceramics sintered at 1300℃. Previous studies have revealed that cells were sensitive to substrate stiffness and surface morphology[51][65].

The cell survival and attachment on the sintered bulk samples after 4 h and 24 h incubation was examined by *in vitro* live/dead assay. As shown in Fig.10A, almost no red fluorescence was shown in the images, indicating that BCP ceramics were significantly biocompatible. After 4 h of incubation, compared to samples sintered at 1100℃, BMSCs presented a better spread cell morphology in the BCP samples sintered at 1200℃ and 1300℃, which indicated that BMSCs could readily adhere on the surface of BCP samples sintered at 1200℃ and 1300℃. After 24 h incubation, BMSCs performed well-spread cell morphology on all samples' surfaces as culture time increased. Besides, as shown in Fig.10B, the SEM observation results implied that BMSCs could maintain cell phenotype and their morphology was well expanded. BMSCs were in a flat and long shape and exhibited stretched morphologies with obvious pseudopodia [Fig.10B(b-f)], demonstrating the sintered BCP ceramics were favorable for cell attachment and adhesion.

3.8 Apatite formation ability

The formation of apatite crystals can predict the *in vivo* bioactivity of the tissue-engineering scaffold [66, 67]. This apatite layer is similar to bone mineral and can easily form chemical bonds with surrounding native tissues. Fig.11 (a,c,e) shows the surface morphology of the sintered BCP ceramics after soaking in the SBF for 3 days.

Obviously, plenty of bone-like apatite was formed on the surface of the sintered ceramics. The SBF solution was oversaturated due to the release of Ca^{2+}, HPO_4^{2-} and PO_4^{3-} ions through dissolution of BCP ceramics and formed nucleation sites on the ceramic surface. The agglomerated apatite crystals were inhomogeneously distributed on the 1100℃-sintered and 1200℃-sintered ceramics (Fig.11 a,c) while the 1300℃-sintered ceramics was completely covered with a uniform layer of apatite crystals on the surface (Fig.11e). This could be explained by the difference of surface morphology of three sintered samples[68]. Fig.11 (b,d,f) shows the chemical composition of these bone-like apatite crystals. Large amounts of Ca, P and O were detected, indicating the calcium phosphate crystals were formed. In addition, small amounts of Mg, Na and Cl were appeared mainly owing to the deposition of the SBF solution[69]. Overall, the apatite formation ability demonstrated the good bioactivities of the sintered bioceramics. The uniform apatite layer formation of the 1300℃-sintered ceramics might have a better interface with native tissues after implantation.

3.9 Fabrication of tissue engineering scaffolds

To verify the fidelity and fabrication freedom of the BCP optimized slurry and printing performance of DLP process, different designs, e.g., porous cubic structures, triply periodic minimal surface (TPMS)-G, 3D scaffolds with triangular and circular pores were designed and fabricated through the DLP printer. The pore sizes ranging from 300 μm to 1mm were successfully obtained, which exhibited the great abilities of processing complex structure with high resolution and accuracy, as shown in

Fig.12. Generally, pore size greater than 300 um is recommended for bone scaffold owing to better vascularization and enhanced new bone formation[70]. Therefore, the fabrication ability in this study could fulfill the suitable pore size and porosity of tissue engineering scaffolds. Besides, it exhibited great competitiveness of design freedom as compared to the published works since various geometries and morphologies could be printed directly. The current study demonstrated the great potential of DLP in constructing complex BCP scaffolds for bone tissue engineering.

4. Conclusions

The nano BCP slurry with high solid loading and low viscosity was prepared and BCP bioceramics were successfully fabricated using DLP AM technology. The powder modification, slurry formulation, and DLP process optimization were systematically investigated. Furthermore, the effects of sintering temperature on the mechanical properties and *in vitro* biological properties of DLP-formed bioceramics were investigated. The conclusions include the following:

1) The optimal dispersant is 9% BYK111 for the surface modification of nano-sized BCP powders (at the HAp:β-TCP ratio of 1:1) to produce photo-curable slurry with high solid loading (65wt.%) as well as low viscosity(400 mPa·s at 50 s^{-1} shear rate level).

2) The optimal photo-initiator concentration is dependent on the energy dose. As the energy dose increases, the location of the optimal photo-initiator concentration

moves forwards lower concentration side.

3) The BCP bioceramic sintered at 1300℃ shows improved mechanical properties as compared to those sintered at 1100℃ or 1200℃. The volume density of the 1300℃-sintered BCP ceramics can reach to 3.037±0.009 g/cm^3 while the hardness is 6.36±0.43GPa. The compressive strength of cubic-shaped porous scaffolds with ~56.3 vol.% porosity is about 20.07±2.09MPa.

4) The BCP ceramics sintered at three respective temperatures show good biocompatibility. Particularly, samples sintered at 1300 ℃ exhibit higher cell proliferation rates, better cell spreading morphology and homogeneous bone-like apatite formation ability.

5) This work has investigated the DLP fabrication of BCP bioceramic and its scaffolds in terms of optimization of slurry formula and sintering process, which could provide a good guidance for preparing high-performance BCP bone scaffolds with high accuracy and good bioactivity using the DLP AM technology. Potentially, the methods and procedures developed in this study may be applied to the DLP fabrication of other ceramics.

Acknowledgments

Y. Wang thanks Southern University of Science and Technology (SUSTech) for providing her with a PhD scholarship in the HKU-SUSTech Joint Education Programme for PhD. This work is supported by Hong Kong's Research Grants Council (RGC) through GRF research grants (17201017, 17200519 and 17202921),

Shenzhen Science and Technology Innovation Commission [Grant No. KQTD20190929172505711], Shenzhen Science and technology International Cooperation programme [Grant No. GJHZ20200731095606021], and the Guangdong Province International Collaboration Programme [Grant No. 2019A050510003]. The authors acknowledge the assistance of SUSTech Core Research Facilities.

References

[1] E. Roddy, M.R. DeBaun, A. Daoud-Gray, Y.P. Yang, M.J. Gardner, Treatment of critical-sized bone defects: clinical and tissue engineering perspectives, European Journal of Orthopaedic Surgery & Traumatology 28(3) (2018) 351-362,https://doi.org/10.1007/s00590-017-2063-0.

[2] A.R. Amini, C.T. Laurencin, S.P. Nukavarapu, Bone tissue engineering: recent advances and challenges, Critical Reviews™ in Biomedical Engineering 40(5) (2012),https://doi.org/10.1615/critrevbiomedeng.v40.i5.10.

[3] A.J. Salgado, O.P. Coutinho, R.L. Reis, Bone tissue engineering: state of the art and future trends, Macromolecular bioscience 4(8) (2004) 743-765,https://doi.org/10.1002/mabi.200400026.

[4] A. Wubneh, E.K. Tsekoura, C. Ayranci, H. Uludağ, Current state of fabrication technologies and materials for bone tissue engineering, Acta Biomaterialia 80 (2018) 1-30,https://doi.org/10.1016/j.actbio.2018.09.031.

[5] P. Deb, A.B. Deoghare, A. Borah, E. Barua, S.D. Lala, Scaffold development using biomaterials: a review, Materials Today: Proceedings 5(5) (2018) 12909-12919,https://doi.org/10.1016/j.matpr.2018.02.276.

[6] H. Qu, H. Fu, Z. Han, Y. Sun, Biomaterials for bone tissue engineering scaffolds: a review, RSC advances 9(45) (2019) 26252-26262,https://doi.org/10.1039/C9RA05214C.

[7] J.-M. Bouler, P. Pilet, O. Gauthier, E. Verron, Biphasic calcium phosphate ceramics for bone reconstruction: a review of biological response, Acta biomaterialia 53 (2017) 1-12,https://doi.org/10.1016/j.actbio.2017.01.076.

[8] G. Daculsi, O. Laboux, O. Malard, P. Weiss, Current state of the art of biphasic calcium phosphate bioceramics, Journal of Materials Science: Materials in Medicine 14(3) (2003) 195-200,https://doi.org/10.1023/A:1022842404495.

[9] Z. Liu, H. Liang, T. Shi, D. Xie, R. Chen, X. Han, L. Shen, C. Wang, Z. Tian, Additive manufacturing of hydroxyapatite bone scaffolds via digital light processing and in vitro compatibility, Ceramics International 45(8) (2019) 11079-11086,https://doi.org/10.1016/j.ceramint.2019.02.195.

[10] C. Feng, K. Zhang, R. He, G. Ding, M. Xia, X. Jin, C. Xie, Additive manufacturing of hydroxyapatite bioceramic scaffolds: Dispersion, digital light processing, sintering, mechanical properties, and biocompatibility, Journal of Advanced Ceramics 9(3) (2020) 360-373,https://doi.org/10.1007/s40145-020-0375-8.

[11] S. Chen, Y. Shi, X. Zhang, J. Ma, Evaluation of BMP-2 and VEGF loaded 3D printed hydroxyapatite composite scaffolds with enhanced osteogenic capacity in vitro and in vivo, Materials Science and Engineering: C 112 (2020) 110893,https://doi.org/10.1016/j.msec.2020.110893.

[12] S. Chen, Y. Shi, X. Zhang, J. Ma, 3D printed hydroxyapatite composite scaffolds with enhanced mechanical properties, Ceramics International 45(8) (2019) 10991-10996,https://doi.org/10.1016/j.ceramint.2019.02.182.

[13] N. Yang, Q. Zhong, Y. Zhou, S.C. Kundu, J. Yao, Y. Cai, Controlled degradation pattern of hydroxyapatite/calcium carbonate composite microspheres, Microscopy Research &Technique 79(6) (2016) 518-24,https://doi.org/10.1002/jemt.22661.

[14] J. Yang, Y. Kang, C. Browne, T. Jiang, Y. Yang, Graded porous β-tricalcium phosphate scaffolds enhance bone regeneration in mandible augmentation, The Journal of craniofacial surgery 26(2) (2015) e148,https://doi.org/10.1097/SCS.0000000000001383.

[15] C. Schmidleithner, S. Malferrari, R. Palgrave, D. Bomze, M. Schwentenwein, D.M. Kalaskar, Application of high resolution DLP stereolithography for fabrication of tricalcium phosphate scaffolds for bone regeneration, Biomedical Materials 14(4) (2019) 045018,https://doi.org/10.1088/1748-605X/ab279d.

[16] L. Caetano Uetanabaro, M. Claudino, R.Z. Mobile, J. Cesar Zielak, G. Pompermaier Garlet, M. Rodrigues de Araujo, Osteoconductivity of Biphasic Calcium Phosphate Ceramic Improves New Bone Formation: A Histologic, Histomorphometric, Gene Expression, and Microcomputed Tomography Study, International Journal of Oral & Maxillofacial Implants 35(1) (2020),http://doi.org/10.11607/jomi.7745.

[17] S.E. Kim, K. Park, Recent Advances of Biphasic Calcium Phosphate Bioceramics for Bone Tissue Regeneration, Biomimicked Biomaterials, Springer2020, pp. 177-188,https://doi.org/10.1007/978-981-15-3262-7_12.

[18] M. Houmard, Q. Fu, M. Genet, E. Saiz, A.P. Tomsia, On the structural, mechanical, and biodegradation properties of HA/β-TCP robocast scaffolds, Journal of Biomedical Materials Research Part B: Applied Biomaterials 101(7) (2013) 1233-1242,http://doi.org/10.1002/jbm.b.32935.

[19] F. Liu, Y. Liu, X. Li, X. Wang, D. Li, S. Chung, C. Chen, I.S. Lee, Osteogenesis of 3D printed macro-pore size biphasic calcium phosphate scaffold in rabbit calvaria, Journal of Biomaterials Applications 33(9) (2019) 1168-1177,https://doi.org/10.1177/0885328218825177.

[20] L. Roseti, V. Parisi, M. Petretta, C. Cavallo, G. Desando, I. Bartolotti, B. Grigolo, Scaffolds for Bone Tissue Engineering: State of the art and new perspectives, Materials Science and Engineering: C 78 (2017) 1246-1262,https://doi.org/10.1016/j.msec.2017.05.017.

[21] A. Haider, S. Haider, M. Rao Kummara, T. Kamal, A.-A.A. Alghyamah, F. Jan Iftikhar, B. Bano, N. Khan, M. Amjid Afridi, S. Soo Han, A. Alrahlah, R. Khan, Advances in the scaffolds fabrication techniques using biocompatible

polymers and their biomedical application: A technical and statistical review, Journal of Saudi Chemical Society 24(2) (2020) 186-215,https://doi.org/10.1016/j.jscs.2020.01.002.

[22] H. Janik, M. Marzec, A review: Fabrication of porous polyurethane scaffolds, Materials Science and Engineering: C 48 (2015) 586-591,https://doi.org/10.1016/j.msec.2014.12.037.

[23] Y. Yang, G. Wang, H. Liang, C. Gao, S. Peng, L. Shen, C. Shuai, Additive manufacturing of bone scaffolds, International Journal of Bioprinting 5(1) (2019),http://doi.org/10.18063/IJB.v5i1.148.

[24] C. Mota, D. Puppi, F. Chiellini, E. Chiellini, Additive manufacturing techniques for the production of tissue engineering constructs, Journal of tissue engineering and regenerative medicine 9(3) (2015) 174-190,https://doi.org/10.1002/term.1635.

[25] S. Giannitelli, P. Mozetic, M. Trombetta, A. Rainer, Combined additive manufacturing approaches in tissue engineering, Acta biomaterialia 24 (2015) 1-11,https://doi.org/10.1016/j.actbio.2015.06.032.

[26] Z. Chen, Z. Li, J. Li, C. Liu, C. Lao, Y. Fu, C. Liu, Y. Li, P. Wang, Y. He, 3D printing of ceramics: A review, Journal of the European Ceramic Society 39(4) (2019) 661-687,https://doi.org/10.1016/j.jeurceramsoc.2018.11.013.

[27] C. Wang, W. Huang, Y. Zhou, L. He, Z. He, Z. Chen, X. He, S. Tian, J. Liao, B. Lu, 3D printing of bone tissue engineering scaffolds, Bioactive materials 5(1) (2020) 82-91,https://doi.org/10.1016/j.bioactmat.2020.01.004.

[28] A. Haleem, M. Javaid, R.H. Khan, R. Suman, 3D printing applications in bone tissue engineering, Journal of clinical orthopaedics and trauma 11 (2020) S118-S124,https://doi.org/10.1016/j.jcot.2019.12.002.

[29] A. Shahzad, I. Lazoglu, Direct ink writing (DIW) of structural and functional ceramics: Recent achievements and future challenges, Composites Part B: Engineering 225 (2021) 109249,https://doi.org/10.1016/j.compositesb.2021.109249.

[30] A.J. Ashwin, J.M. Jafferson, State of the art direct ink writing (DIW) and experimental trial on DIW of HAp bio-ceramics, Materials Today: Proceedings 46 (2021) 1298-1307,https://doi.org/10.1016/j.matpr.2021.02.396.

[31] D. Belgin Paul, A. Praveen, U. Golcha, Extrusion Based 3D-Printing of Bioceramic Structures-A Review, Composite Materials for Extreme Loading (2022) 221-231,http://doi.org/10.1007/978-981-16-4138-1_17.

[32] N. Beheshtizadeh, M. Azami, H. Abbasi, A. Farzin, Applying extrusion-based 3D printing technique accelerates fabricating complex biphasic calcium phosphate-based scaffolds for bone tissue regeneration, Journal of Advanced

Research (2021),https://doi.org/10.1016/j.jare.2021.12.012.

[33] M.H. Monfared, A. Nemati, F. Loghman, M. Ghasemian, A. Farzin, N. Beheshtizadeh, M. Azami, A deep insight into the preparation of ceramic bone scaffolds utilizing robocasting technique, Ceramics International 48(5) (2022) 5939-5954,https://doi.org/10.1016/j.ceramint.2021.11.268.

[34] F.P. Melchels, J. Feijen, D.W. Grijpma, A review on stereolithography and its applications in biomedical engineering, Biomaterials 31(24) (2010) 6121-6130,https://doi.org/10.1016/j.biomaterials.2010.04.050.

[35] J. Zhang, Q. Hu, S. Wang, J. Tao, M. Gou, Digital Light Processing Based Three-dimensional Printing for Medical Applications, International Journal of Bioprinting 6 (2020),https://doi.org/10.18063/ijb.v6i1.242.

[36] S. Zakeri, M. Vippola, E. Levänen, A comprehensive review of the photopolymerization of ceramic resins used in stereolithography, Additive Manufacturing 35 (2020) 101177,https://doi.org/10.1016/j.addma.2020.101177.

[37] H. Liang, Y. Wang, S. Chen, Y. Liu, Z. Liu, J. Bai, Nano-Hydroxyapatite Bone Scaffolds with Different Porous Structures Processed by Digital Light Processing 3D Printing, International Journal of Bioprinting, 2022 8(1) (2022),http://doi.org/10.18063/ijb.v8i1.502.

[38] H. Li, Y. Liu, Y. Liu, J. Wang, Q. Zeng, K. Hu, Z. Lu, Influence of vacuum debinding temperature on microstructure and mechanical properties of three-dimensional-printed alumina via stereolithography, 3D Printing and Additive Manufacturing 7(1) (2020) 8-18,https://doi.org/10.1089/3dp.2019.0060.

[39] K. Zhang, Q. Meng, X. Zhang, Z. Qu, S. Jing, R. He, Roles of solid loading in stereolithography additive manufacturing of ZrO2 ceramic, International Journal of Refractory Metals and Hard Materials (2021) 105604,https://doi.org/10.1016/j.ijrmhm.2021.105604.

[40] J. Sun, J. Binner, J. Bai, 3D printing of zirconia via digital light processing: optimization of slurry and debinding process, Journal of the European Ceramic Society 40(15) (2020) 5837-5844,https://doi.org/10.1016/j.jeurceramsoc.2020.05.079.

[41] H. Wu, Y. Cheng, W. Liu, R. He, M. Zhou, S. Wu, X. Song, Y. Chen, Effect of the particle size and the debinding process on the density of alumina ceramics fabricated by 3D printing based on stereolithography, Ceramics International 42(15) (2016) 17290-17294,https://doi.org/10.1016/j.ceramint.2016.08.024.

[42] Z. Chen, J. Li, C. Liu, Y. Liu, J. Zhu, C. Lao, Preparation of high solid loading and low viscosity ceramic slurries for photopolymerization-based 3D printing, Ceramics International 45(9) (2019) 11549-11557,https://doi.org/10.1016/j.ceramint.2019.03.024.

[43] G. Mitteramskogler, R. Gmeiner, R. Felzmann, S. Gruber, C. Hofstetter, J. Stampfl, J. Ebert, W. Wachter, J. Laubersheimer, Light curing strategies for lithography-based additive manufacturing of customized ceramics, Additive Manufacturing 1 (2014) 110-118,https://doi.org/10.1016/j.addma.2014.08.003.

[44] S.-E. Bendaoudi, M. Bounazef, A. Djeffal, The effect of sintering temperature on the porosity and compressive strength of corundum, Journal of the Mechanical Behavior of Materials 27(3-4) (2018),https://doi.org/10.1515/jmbm-2018-0018.

[45] R. LeGeros, S. Lin, R. Rohanizadeh, D. Mijares, J. LeGeros, Biphasic calcium phosphate bioceramics: preparation, properties and applications, Journal of materials science: Materials in Medicine 14(3) (2003) 201-209,https://doi.org/10.1023/A:1022872421333.

[46] O. Brown, M. McAfee, S. Clarke, F. Buchanan, Sintering of biphasic calcium phosphates, Journal of Materials Science: Materials in Medicine 21(8) (2010) 2271-2279,https://doi.org/10.1007/s10856-010-4032-6.

[47] H. Chen, W. Dou, Q. Zhu, D. Jiang, J. Xia, X. Wang, W. Tang, S. Wang, The extraction and characterization of porous HA/β-TCP biphasic calcium phosphate from sole fish bones at different temperatures, Materials Research Express 6(12) (2019) 125412,http://dx.doi.org/10.1088/2053-1591/ab5a8f.

[48] V. Uskoković, J.V. Rau, Nonlinear oscillatory dynamics of the hardening of calcium phosphate bone cements, RSC advances 7(64) (2017) 40517-40532,http://doi.org/10.1039/C7RA07395J.

[49] J. Sun, X. Chen, J. Wade-Zhu, J. Binner, J. Bai, A comprehensive study of dense zirconia components fabricated by additive manufacturing, Additive Manufacturing 43 (2021) 101994,https://doi.org/10.1016/j.addma.2021.101994.

[50] A. Bagheri Saed, A.H. Behravesh, S. Hasannia, S.A. Alavinasab Ardebili, B. Akhoundi, M. Pourghayoumi, Functionalized poly l-lactic acid synthesis and optimization of process parameters for 3D printing of porous scaffolds via digital light processing (DLP) method, Journal of Manufacturing Processes 56 (2020) 550-561,https://doi.org/10.1016/j.jmapro.2020.04.076.

[51] S.Y. Song, M.S. Park, D. Lee, J.W. Lee, J.S. Yun, Optimization and characterization of high-viscosity ZrO2 ceramic nanocomposite resins for supportless stereolithography, Materials & Design 180 (2019) 107960,https://doi.org/10.1016/j.matdes.2019.107960.

[52] J. Sun, J. Binner, J. Bai, Effect of surface treatment on the dispersion of nano zirconia particles in non-aqueous suspensions for stereolithography, Journal of the European Ceramic Society 39(4) (2019) 1660-1667,https://doi.org/10.1016/j.jeurceramsoc.2018.10.024.

[53] W. Wang, J. Sun, B. Guo, X. Chen, K.P. Ananth, J. Bai, Fabrication of

piezoelectric nano-ceramics via stereolithography of low viscous and non-aqueous suspensions, Journal of the European Ceramic Society 40(3) (2020) 682-688,https://doi.org/10.1016/j.jeurceramsoc.2019.10.033.

[54] D. Gardini, M. Deluca, M. Nagliati, C. Galassi, Flow properties of PLZTN aqueous suspensions for tape casting, Ceramics International 36(5) (2010) 1687-1696,https://doi.org/10.1016/j.ceramint.2010.03.011.

[55] J.H. Lee, R.K. Prud'Homme, I.A. Aksay, Cure depth in photopolymerization: Experiments and theory, Journal of Materials Research 16(12) (2001) 3536-3544,https://doi.org/10.1557/JMR.2001.0485.

[56] Y. Wei, D. Zhao, Q. Cao, J. Wang, Y. Wu, B. Yuan, X. Li, X. Chen, Y. Zhou, X. Yang, Stereolithography-based additive manufacturing of high-performance osteoinductive calcium phosphate ceramics by a digital light-processing system, ACS Biomaterials Science & Engineering 6(3) (2020) 1787-1797,https://doi.org/10.1021/acsbiomaterials.9b01663.

[57] C. Zhang, Z. Luo, C. Liu, J. Zhu, J. Cao, J. Yuan, P. Wang, C. Liu, C. Lao, Z. Chen, Dimensional retention of photocured ceramic units during 3D printing and sintering processes, Ceramics International 47(8) (2021) 11097-11108,https://doi.org/10.1016/j.ceramint.2020.12.233.

[58] D.D. Deligianni, N.D. Katsala, P.G. Koutsoukos, Y.F. Missirlis, Effect of surface roughness of hydroxyapatite on human bone marrow cell adhesion, proliferation, differentiation and detachment strength, Biomaterials 22(1) (2000) 87-96,https://doi.org/10.1016/S0142-9612(00)00174-5.

[59] Y. Hou, L. Yu, W. Xie, L.C. Camacho, M. Zhang, Z. Chu, Q. Wei, R. Haag, Surface roughness and substrate stiffness synergize to drive cellular mechanoresponse, Nano letters 20(1) (2019) 748-757,https://doi.org/10.1021/acs.nanolett.9b04761.

[60] H.-I. Chang, Y. Wang, Cell responses to surface and architecture of tissue engineering scaffolds, Regenerative medicine and tissue engineering-cells and biomaterials, InTechOpen2011,https://doi.org/10.5772/837.

[61] K. Hatano, H. Inoue, T. Kojo, T. Matsunaga, T. Tsujisawa, C. Uchiyama, Y. Uchida, Effect of surface roughness on proliferation and alkaline phosphatase expression of rat calvarial cells cultured on polystyrene, Bone 25(4) (1999) 439-45,https://doi.org/10.1016/S8756-3282(99)00192-1.

[62] J.-W. Lee, Y.-H. Lee, H. Lee, Y.-H. Koh, H.-E. Kim, Improving mechanical properties of porous calcium phosphate scaffolds by constructing elongated gyroid structures using digital light processing, Ceramics International 47(3) (2021) 3252-3258,https://doi.org/10.1016/j.ceramint.2020.09.164.

[63] R.G. Carrodeguas, S. De Aza, α-Tricalcium phosphate: Synthesis, properties and biomedical applications, Acta Biomaterialia 7(10) (2011) 3536-3546,https://doi.org/10.1016/j.actbio.2011.06.019.

[64] M.-P. Ginebra, E.B. Montufar, 9 - Cements as bone repair materials, in: K.M. Pawelec, J.A. Planell (Eds.), Bone Repair Biomaterials (Second Edition), Woodhead Publishing2019, pp. 233-271,https://doi.org/10.1016/B978-0-08-102451-5.00009-3.

[65] C.B. Khatiwala, S.R. Peyton, A.J. Putnam, Intrinsic mechanical properties of the extracellular matrix affect the behavior of pre-osteoblastic MC3T3-E1 cells, American Journal of Physiology-Cell Physiology 290(6) (2006) C1640-C1650,https://doi.org/10.1152/ajpcell.00455.2005.

[66] A.A. Zadpoor, Relationship between in vitro apatite-forming ability measured using simulated body fluid and in vivo bioactivity of biomaterials, Materials Science and Engineering: C 35 (2014) 134-143,https://doi.org/10.1016/j.msec.2013.10.026.

[67] T. Kokubo, H. Takadama, Simulated body fluid (SBF) as a standard tool to test the bioactivity of implants, Handbook of biomineralization: biological aspects and structure formation (2007) 97-109,https://doi.org/10.1002/9783527619443.ch51.

[68] H. Qu, M. Wei, The effect of temperature and initial pH on biomimetic apatite coating, Journal of Biomedical Materials Research Part B: Applied Biomaterials: An Official Journal of The Society for Biomaterials, The Japanese Society for Biomaterials, and The Australian Society for Biomaterials and the Korean Society for Biomaterials 87(1) (2008) 204-212,https://doi.org/10.1002/jbm.b.31096.

[69] H.M. Kim, T. Himeno, M. Kawashita, T. Kokubo, T. Nakamura, The mechanism of biomineralization of bone-like apatite on synthetic hydroxyapatite: an in vitro assessment, Journal of the Royal Society Interface 1(1) (2004) 17-22,https://doi.org/10.1098/rsif.2004.0003.

[70] V. Karageorgiou, D. Kaplan, Porosity of 3D biomaterial scaffolds and osteogenesis, Biomaterials 26(27) (2005) 5474-91,https://doi.org/10.1016/j.biomaterials.2005.02.002.

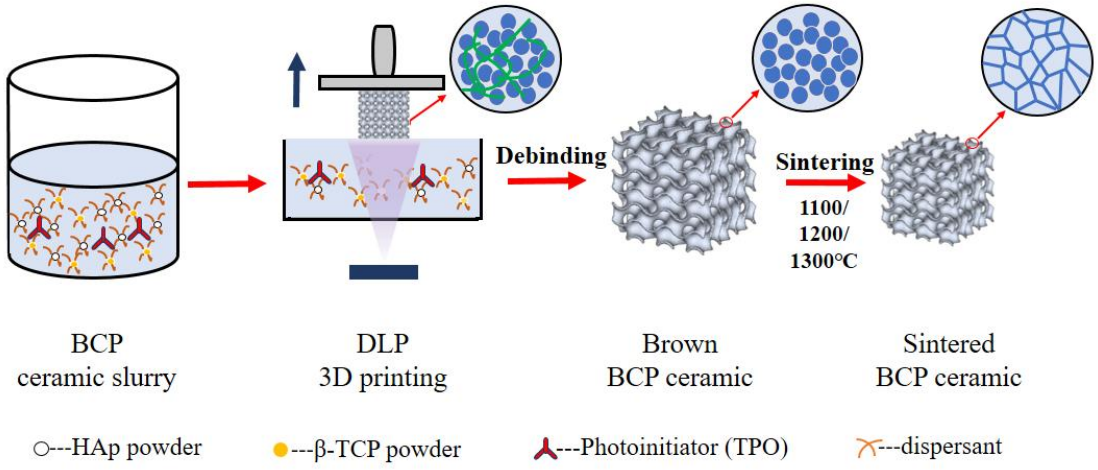

Fig.1. Schematic illustration for BCP ceramic scaffold fabrication via DLP.

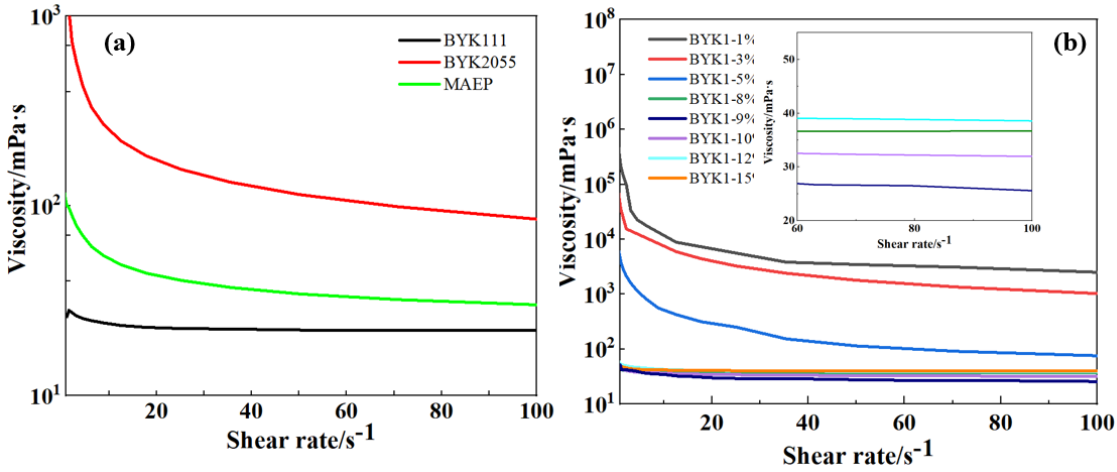

Fig.2 Effects of (a) three different types of dispersants and (b) BYK111 with different concentrations on viscosities of 40 wt. % BCP ceramic slurry.

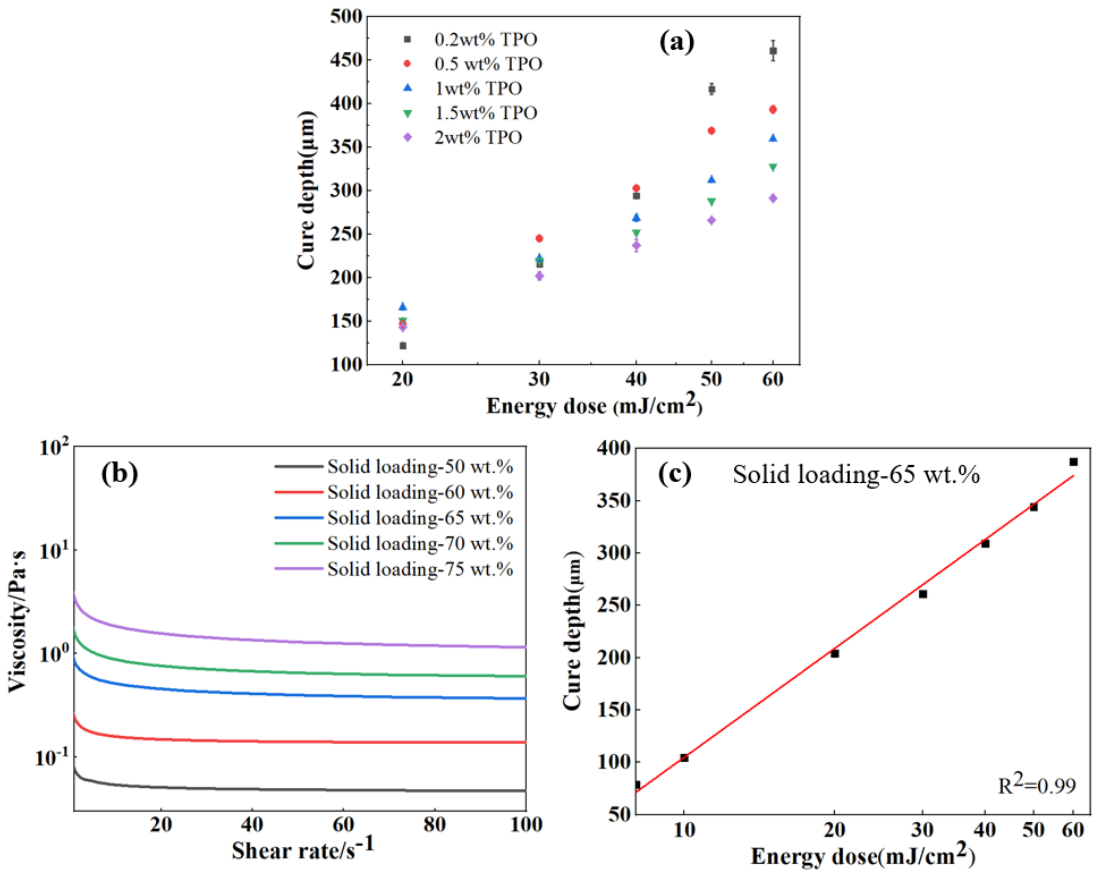

Fig.3. (a) Effects of TPO concentration and energy dose on cure depth; (b) Viscosities of BCP slurries with different solid loading; (c) The relation of cure depth and energy dose of slurry with 65 wt.% BCP.

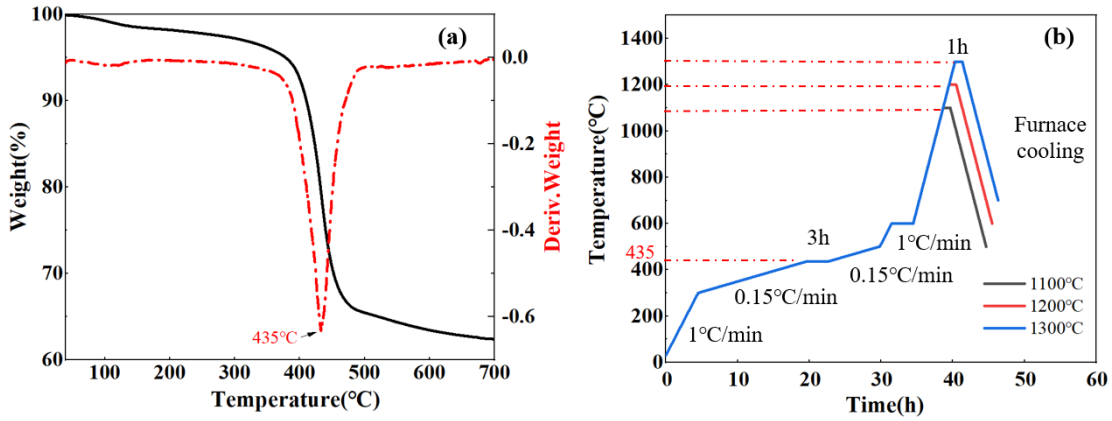

Fig.4. (a) TGA/DTG curve of green part; (b) debinding and sintering profile.

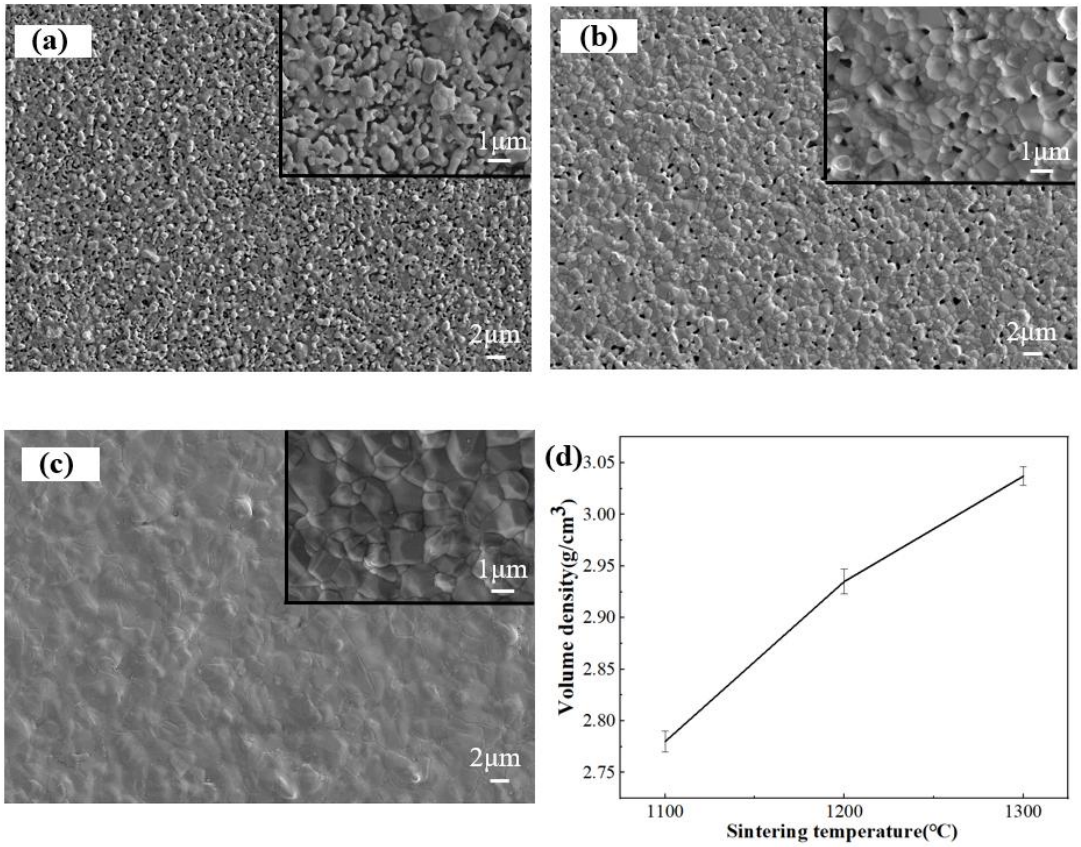

Fig.5. Microstructures of samples after sintering at (a) 1100℃; (b) 1200℃; (c) 1300℃. (d) Volume density of samples after sintering 1100-1300℃.

	Top Surface		Bottom Surface	
	3D images	Sa(μm)	3D images	Sa(μm)
Sintering -1100	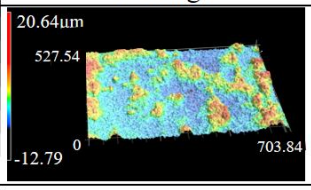	2.53±0.16	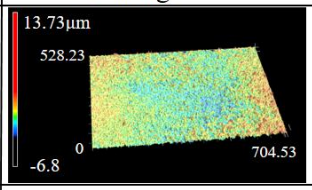	0.83±0.08
Sintering -1200	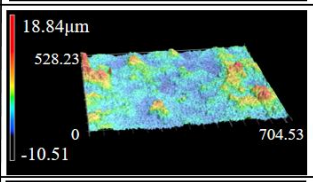	2.31±0.16	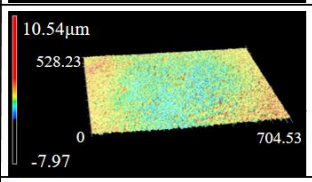	0.77±0.10
Sintering -1300	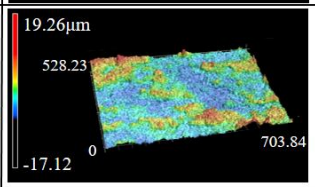	2.31±0.16	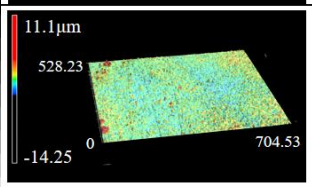	0.75±0.01

Fig.6. 3D topography and surface roughness of the sintered BCP parts

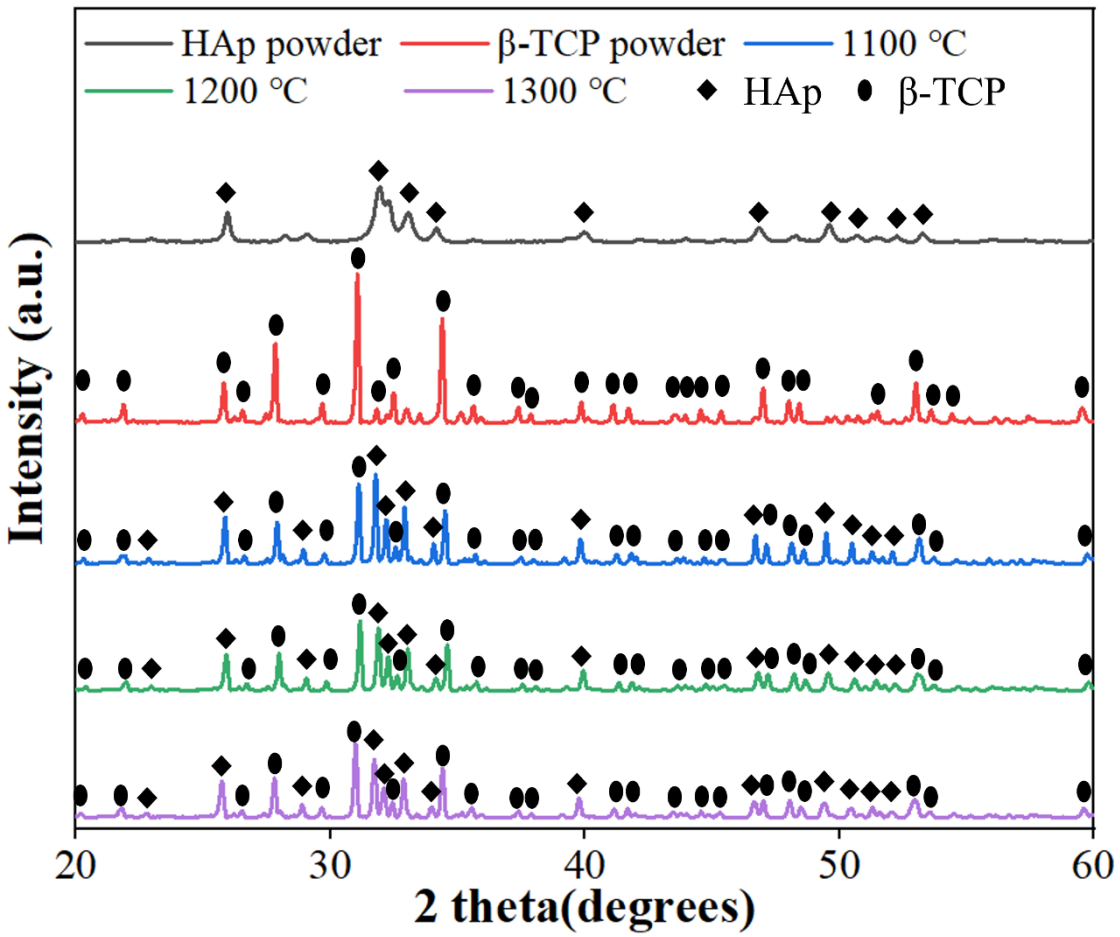

Fig.7. XRD pattern of sintered BCP ceramics after sintering at 1100℃, 1200℃, and 1300℃.

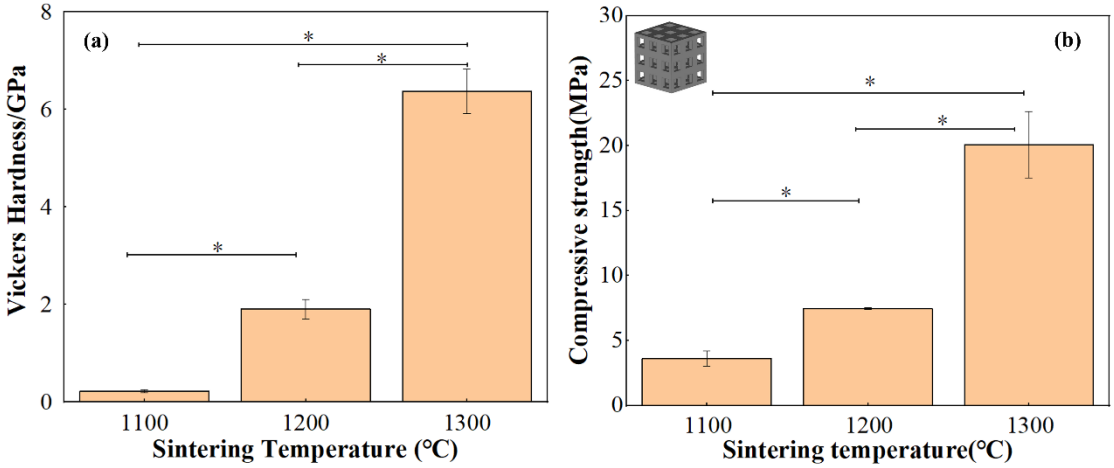

Fig.8. Mechanical properties of sintered BCP ceramics: (a) Vickers hardness; (b) Compressive strength of scaffolds (* represents P<0.05)

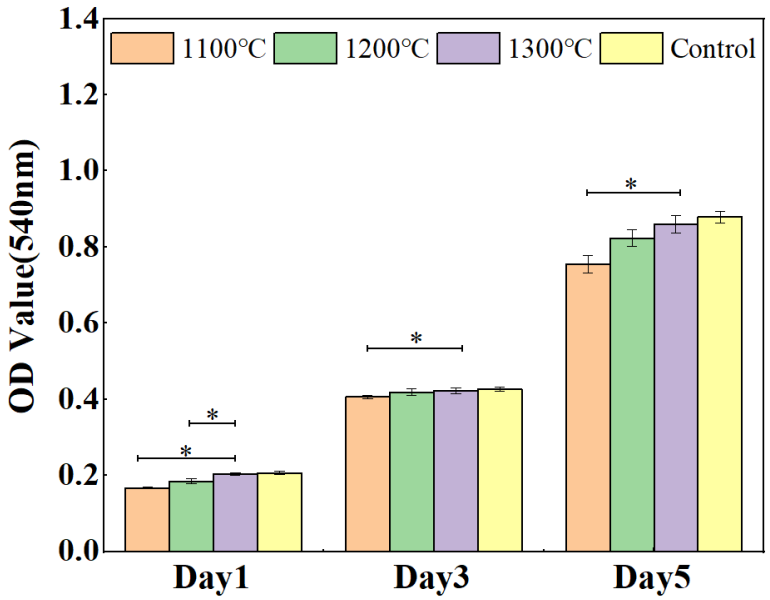

Fig.9. Results of MTT assay of BMSCs cultured on the DLP-formed BCP ceramics (* represents P<0.05)

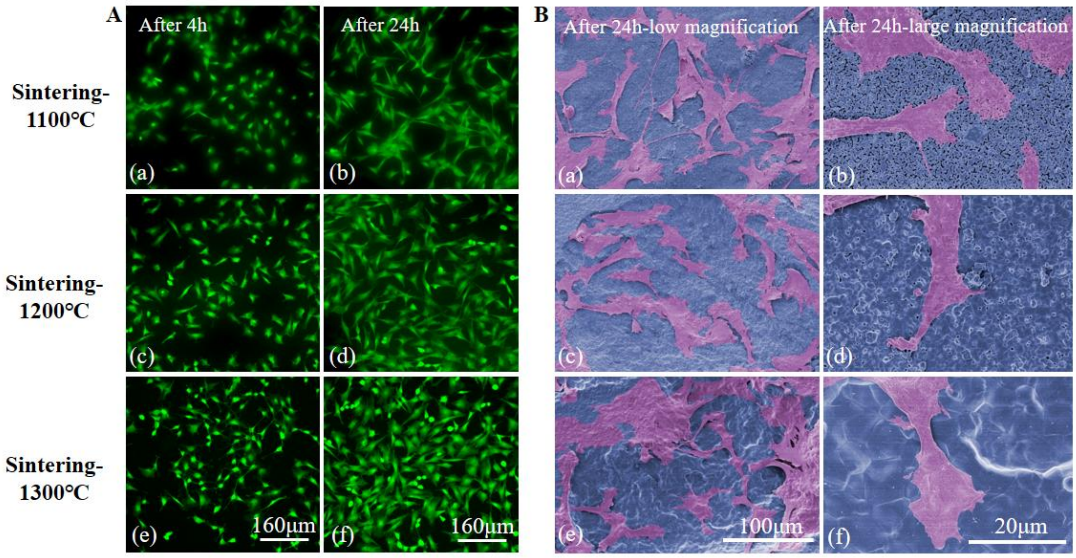

Fig.10 *In vitro* biological responses on three groups of sintered BCP ceramics: A. fluorescence images of BMSCs live/dead staining after cultured for 4h and 24h; B. SEM images of BMSCs morphology after cultured for 24h.

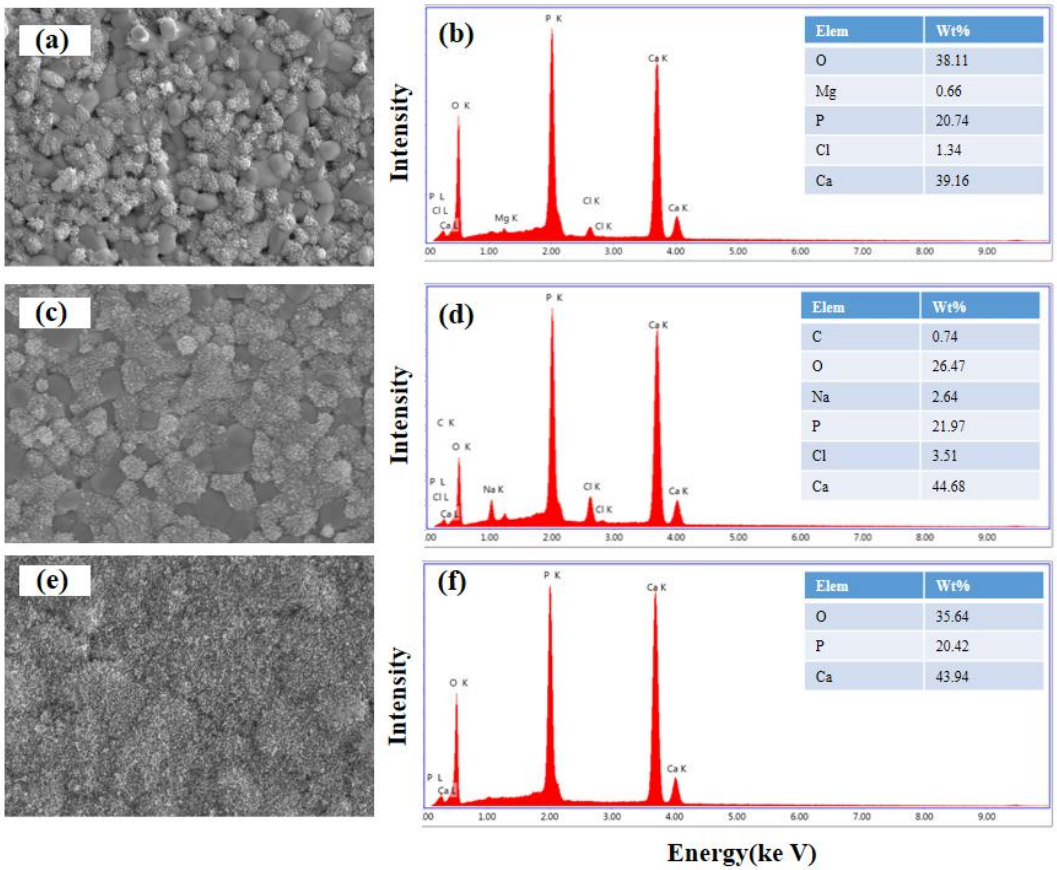

Fig.11 SEM images and EDS analysis of bone-like apatite formed on sintered BCP ceramics after soaking in SBF for 3 days: (a-b) 1100℃; (c-d) 1200℃; (e-f) 1300℃

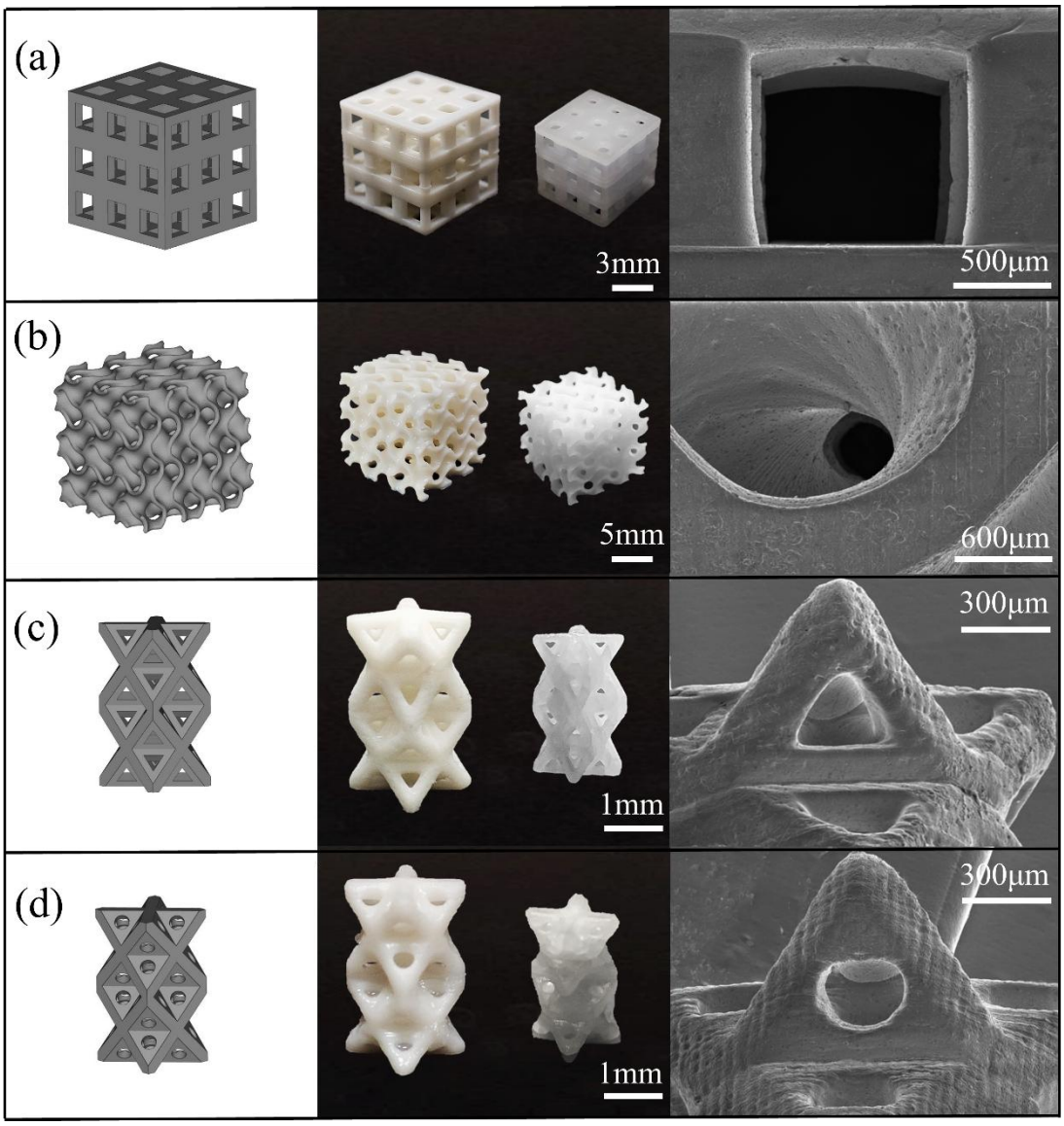

Fig.12. 3D models (left column), green bodies, 1300°C-sintered BCP scaffolds (middle column), and SEM images of various scaffolds (right column): (a) cubic (used for compression test); (b) TPMS-G; (c-d) 3D scaffolds with triangular and circular pores.

Table 1. Shrinkages of DLP-formed BCP ceramics

Material	X-Y direction		Z direction	
	Diameter/mm	Shrinkage/%	Thickness/mm	Shrinkage/%
Design	10		1	
Green body	10.37±0.05		1.08±0.03	
1100°C sintering	9.35±0.08	6.5	0.94±0.01	6.0
1200°C sintering	8.38±0.02	16.2	0.83±0.01	17.0
1300°C sintering	7.76±0.03	22.4	0.78±0.01	22.0